Measurements of ^{3}He spin-exchange rates

B. Chann, E. Babcock, L. W. Anderson, and T. G. Walker
Department of Physics, University of Wisconsin-Madison, Madison, Wisconsin 53706
(Received 27 February 2002; published 13 September 2002)

Spin-exchange rate coefficients for Rb-^{3}He are measured using three different methods. Two methods, using Rb repolarization and rate balance, require no assumption about the nature of the ^{3}He wall relaxation and agree well; we find spin-exchange rate coefficients of 6.7×10^{-20} cm^3/s and 6.8×10^{-20} cm^3/s. These results agree with a recent repolarization measurement of Baranga and co-workers [Phys. Rev. Lett. **80**, 2801 (1998)]. The third method uses the temperature dependence of the ^{3}He relaxation and is 30% larger than the other two, implying a temperature-dependent wall or an unreasonably large value of the anisotropic spin-exchange interaction for Rb-^{3}He. In the course of these measurements we developed and tested a new method for Rb density measurements under high power pumping conditions, and a new variant of Rb EPR polarimetry, both of which are described here.

DOI: 10.1103/PhysRevA.66.032703 PACS number(s): 34.30.+h, 32.80.Bx, 33.25.+k

I. INTRODUCTION

Hyperpolarized ^{3}He gas is currently being applied to a wide variety of scientific and medical problems. These include magnetic resonance imaging [1,2], spin-polarized targets [3], polarized neutrons [4], and precision measurements [5]. All of these applications would benefit from being able to produce ^{3}He polarizations in excess of 90%. Given the current knowledge of the fundamental spin-exchange and spin-relaxation rates for Rb-^{3}He, and the existence of long-lifetime room-temperature ^{3}He storage cells [6,7], it should be possible to acheive such polarizations using spin-exchange optical pumping [8]. Such high polarizations have not been attained, however, and indeed with few exceptions [9–11] polarizations over 55% have not been reported. A second technology, metastability-exchange optical pumping, has been shown to give polarizations up to 85% at low pressures [12]. The use of compression methods has enabled polarizations of high-density ^{3}He of typically 50% [13,14].

Until the recent work of Baranga *et al.* [15], only two measurements of the most fundamental parameter of Rb-^{3}He spin exchange, the spin-exchange rate coefficient, had been reported. Coulter and co-workers [16] measured the relaxation times of ^{3}He as a function of temperature, and from that dependence deduced a value of $1.2\pm0.2\times10^{-19}$ cm^3/s for the spin-exchange rate coefficient. Larson *et al.* [10] used a similar method and obtained $6.2\pm0.2\times10^{-20}$ cm^3/s, nearly a factor of 2 smaller. Both these experiments deduced the Rb vapor pressure using published saturated vapor pressure curves, a procedure that can be in error by a factor of 2 or more. In addition, the assumption must be made that the ^{3}He relaxation rate due to processes other than spin exchange is temperature independent. In particular, differing temperature-dependent wall relaxation rates could account for the difference. Recently, Baranga *et al.* [15] deduced a spin-exchange rate coefficient of 6.7×10^{-20} cm^3/s by measuring the absolute Rb polarization induced by spin exchange from ^{3}He of a known polarization. This method requires no measurement of the Rb density, and makes no assumptions about the wall relaxation. It should therefore be quite reliable.

In order to better understand the discrepancies between these three experiments, and to further test our basic understanding of the spin-exchange optical pumping process so as to isolate those effects that limit the ^{3}He polarizations, in this paper we present measurements of the spin-exchange rate coefficient using both previous methods (Rb density dependence of ^{3}He relaxation, Rb repolarization) and a new ''rate-balance'' method based on the equilibrium ^{3}He polarization attained in a cell of known Rb density and polarization.

Section II presents the various methods and emphasizes their underlying assumptions. The rate-balance method, such as the repolarization method, makes no assumptions about the nature of the ^{3}He relaxation and, in particular, does not require an understanding of how the wall relaxation depends on temperature.

Section III is a description of the experiment, emphasizing the redundant methods we have used to assure the accuracy of our determination of the crucial parameters of Rb density, Rb polarization, and He polarization. Included in this discussion is a description of a method for determining the Rb density in the presence of intense optical pumping light, and our new variant of Rb polarimetry.

In Sec. IV we present and discuss the results. We find that the rate-balance and repolarization methods agree very well with each other and with the Baranga *et al.* repolarization result, but the ^{3}He relaxation rate method gives a value about 30% higher. The discrepancy can be reconciled by assuming either that the wall-relaxation rate is temperature dependent with an Arrhenius temperature comparable to that of the Rb vapor pressure, or by assuming that anisotropic spin exchange, believed on theoretical grounds to be negligible [17], is present at a very significant level. We present arguments for a temperature-dependent wall, but further experiments will be required to distinguish between these possibilities.

II. THEORY

The fundamental rate equation governing polarization of ^{3}He by spin-exchange collisions with rubidium atoms of density [Rb] is

$$\frac{dP_{\mathrm{He}}}{dt} = k_a[\mathrm{Rb}](\overline{P_{\mathrm{Rb}} - P_{\mathrm{He}}}) - \Gamma_w P_{\mathrm{He}} + k_b[\mathrm{Rb}](\overline{-P_{\mathrm{Rb}}/2} - P_{\mathrm{He}}). \quad (1)$$

The first two terms are well known [8,18], and represent Rb-^{3}He spin-exchange collisions (rate coefficient k_a) and ^{3}He wall relaxation. Spin-exchange arises from the short-range Fermi contact hyperfine interaction $\alpha \mathbf{S}\cdot\mathbf{K}$ that is present during binary collisions between the spin-polarized alkali atoms of spin $\mathbf{S}$ and the ^{3}He atoms of nuclear spin $\mathbf{K}$. It is convenient to introduce the longitudinal spin-polarizations $P_{\mathrm{He}} = 2\langle K_z\rangle$ and $P_{\mathrm{Rb}} = 2\langle S_z\rangle$, with the z direction being that of the applied static magnetic field. The interaction of ^{3}He with well-prepared container walls is weak, so the ''wall-relaxation'' rate Γ_w is small as compared to the diffusion rates. In this limit there exist only tiny gradients of P_{He} across the cell and so the ^{3}He atoms sample the volume-averaged alkali spin polarization $\overline{P_{\mathrm{Rb}}}$. The relaxation due to He-He collisions [19] is quite small in our experiment and is lumped into Γ_w.

The third term in Eq. (1) represents spin transfer (rate coefficient k_b) to the ^{3}He nucleus from the anisotropic hyperfine interaction $B\mathbf{S}\cdot(3\hat{\mathbf{R}}\hat{\mathbf{R}} - 1)\cdot\mathbf{K}$, $\mathbf{R}$ being the displacement vector between the two colliding atoms. This interaction is produced by the precession of the ^{3}He magnetic moment about the long-range part of the magnetic field produced by the Rb electron. The anisotropic hyperfine interaction has only recently been considered in some theoretical detail [17], and estimates suggest that it should be small compared to normal spin-exchange. However, this has not been tested experimentally, so we will make no assumptions about the relative size of the two terms that contribute to spin transfer between alkali atoms and ^{3}He. Note from Eq. (1) that the anisotropic hyperfine interaction tends to polarize the ^{3}He spin antiparallel to the alkali spin [17].

From Eq. (1), the time constant for buildup or decay of the ^{3}He polarization is

$$\Gamma_{\mathrm{He}} = (k_a + k_b)[\mathrm{Rb}] + \Gamma_w. \quad (2)$$

In a steady state, the ^{3}He polarization is

$$P_{\mathrm{He}} = \frac{(k_a - k_b/2)[\mathrm{Rb}]}{\Gamma_{\mathrm{He}}}\overline{P_{\mathrm{Rb}}}. \quad (3)$$

These two equations suggest two methods for measuring the spin-exchange rate coefficients. The first method, which we will call the relaxation-rate method, is to measure Γ_{He} as a function of $[\mathrm{Rb}]$, the slope of such a plot being $k_a + k_b$. This method has been used previously [10,16], and relies on the assumption that the wall relaxation rate is temperature-independent. It also requires a reliable measurement of the Rb density.

The second method, first used in this work and termed the rate-balance method, uses Eq. (3):

$$k_a - k_b/2 = \frac{P_{\mathrm{He}}\Gamma_{\mathrm{He}}}{\overline{P_{\mathrm{Rb}}}[\mathrm{Rb}]}. \quad (4)$$

Each of the four quantities on the right-hand side of this equation must be measured to obtain the spin-transfer rates. A key point is that in doing so no assumption is made about the nature of the ^{3}He relaxation. In particular, a temperature-dependent wall-relaxation rate affects both Γ_{He} and P_{He} such that their product in Eq. (3) remains the same. An equivalent method, suggested by Gentile, would be to measure $dP_{\mathrm{He}}/dt = (k_a - k_b/2)[\mathrm{Rb}]\,\overline{P_{\mathrm{Rb}}}$ at $P_{\mathrm{He}} = 0$.

A third repolarization method for obtaining the spin-transfer rate coefficients was recently introduced by Baranga *et al.* [15]. In the absence of optical pumping (identified with 0 subscripts), the Rb total longitudinal spin $\langle F_z\rangle_0 = \langle I_z\rangle_0 + \langle S_z\rangle_0$, where $\langle I_z\rangle$ is the Rb longitudinal nuclear spin, obeys

$$\frac{d\langle F_z\rangle_0}{dt} = D\nabla^2\langle F_z\rangle_0 - \Gamma_{\mathrm{Rb}}\langle S_z\rangle_0 + k_a[\mathrm{He}](\langle K_z\rangle - \langle S_z\rangle_0) + k_b[\mathrm{He}](-\langle K_z\rangle/2 - \langle S_z\rangle_0). \quad (5)$$

The first and second terms represent diffusion D and collision losses (Γ_{Rb}, assumed to be solely by electron randomization) for the Rb atoms, while the other terms are the spin-transfer terms analogous to Eq. (1). As long as the collisional losses are much greater than the diffusion losses, we can neglect diffusion (or make a small correction) and find for $\Gamma_{\mathrm{Rb}} \gg (k_a + k_b)[\mathrm{He}]$,

$$k_a - k_b/2 = \frac{\Gamma_{\mathrm{Rb}} P_{\mathrm{Rb0}}}{P_{\mathrm{He0}}[\mathrm{He}]}. \quad (6)$$

Physically, this is simply a statement that the Rb polarization attained with the optical pumping is a balance between the rate at which the Rb atoms are polarized by spin-exchange collisions with the polarized ^{3}He, and the rate at which that polarization is destroyed due to collisions. Like the rate-balance method, the repolarization method makes no assumption about the wall relaxation, and in fact has the additional advantage of requiring no $[\mathrm{Rb}]$ measurement. The assumption that the Rb spin relaxation is dominated by electron randomization is discussed in the Appendix.

In summary, we have three different methods for determining the spin-exchange rate coefficient. An important point is to note that they measure different combinations of the fundamental rate coefficients k_a and k_b for isotropic and anisotropic spin exchange. The rate-balance and repolarization methods measure the combination $k_a - k_b/2$, while the relaxation-rate method gives $k_a + k_b$. In the absence of anisotropic spin exchange the three methods will agree. But if anisotropic spin exchange is important the relaxation rate method will give different results than the others. However, the relaxation method can also be contaminated by wall relaxation that can mimic a nonzero k_b. Having described the three methods for measuring the spin-exchange rate coefficients, we turn now to a description of the experiment.

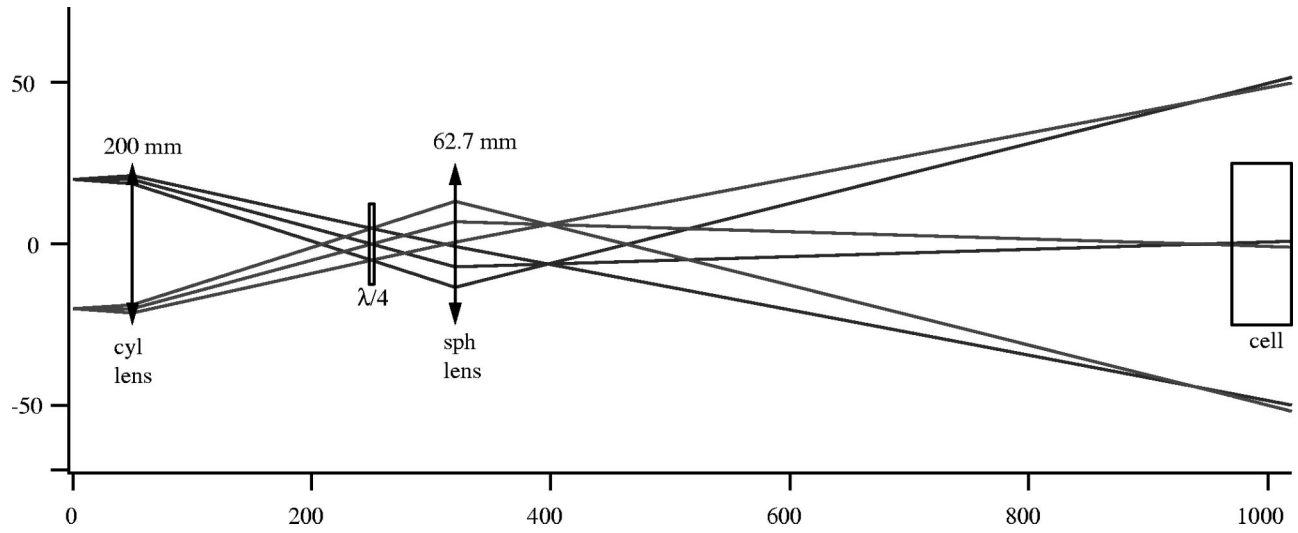

FIG. 1. Optical system for coupling to cell. The laser consists of 20 emitters, rays from two of them are shown. A cylindrical transform lens provides a roughly uniform intensity beam at the λ/4 plate that is imaged onto the cell. The cell is substantially overfilled to ensure uniform optical pumping. Distances are in millimeters.

III. EXPERIMENT

The spin-exchange rate coefficient measurements require careful and absolute determination of Rb densities, polarizations, and relaxation rates, as well as ^{3}He polarization and relaxation rates. We measure the Rb densities in three different ways: field-dependent Faraday rotation [20,21], polarization Faraday rotation, and absorption spectroscopy on the second resonance line of Rb. Rb polarimetry is performed with a variant of the rf-spectroscopic method recently introduced by Young and co-workers [22,23]. The Rb relaxation rate is measured with a weak probe beam by observing Rb polarization transients at low Rb polarization. The ^{3}He polarization is measured using the frequency shift of the Rb rf transitions produced by the effective magnetic field of the polarized ^{3}He [24], and the ^{3}He relaxation rate is measured by observing the long-term decay of the amplitude of repeated free-induction-decay transients. We begin this section with a general discussion of the apparatus and the Faraday rotation method used for many of these diagnostics, and then discuss each of the diagnostics in turn.

A. General features

In order to have a system as carefully characterized as possible, we have used for this experiment an optically sealed cylindrical cell manufactured and generously provided to us by Gentile and colleagues at the National Institute of Standards and Technology (NIST). The NIST cell construction has been described in detail elsewhere [7]; its body is made from Corning 1720 glass and the windows are made of GE180 glass. Its has a room-temperature relaxation rate of about 250 h. It contains 0.77 amagat of ^{3}He, 0.08 amagat of N_2 for radiative quenching of the optically pumped Rb, and a small amount of Rb metal. It measures $l = 4.9$ cm in length and $2a = 4.5$ cm in inner diameter. The cell is heated with hot air; its surface temperature is stabilized to better than 1°C, measured by observing a small piece of blackened metallic tape with an optical pyrometer. The pyrometer was calibrated against a thermocouple that was temporarily taped to the cell and then removed during the ^{3}He polarization experiments.

The magnetic field, typically of 2–8 G, is generated by a 135-turn, 1-m-diameter Helmholtz coil driven by a dc power supply. For short periods of time the field can be increased to as high as 35 G as needed to resolve rf transitions for Rb polarimetry. The magnetic field is stabilized by feedback from a fluxgate magnetometer to a level of 100 μG. Ten additional turns on the field coils are used for shimming magnetic-field gradients.

The laser source for optical pumping was a frequency narrowed diode laser bar [25] (Coherent p/n B1-40C-19-30-A, selected for a small curvature in the alignment of the optical elements) that provides 15 W within a 125-GHz bandwidth at the Rb $5S_{1/2} \rightarrow 5P_{1/2}$ resonance at 795 nm. The high, spatially asymmetric output (19 emitters in a 5 cm $\times$0.5 cm area) of this laser is efficiently coupled to the cell using the optical system as shown in Fig. 1. A 200-mm cylindrical transform lens produces a symmetric, uniform beam on the λ/4 plate. A spherical lens then images this plane onto the front face of the cell.

B. Faraday rotation diagnostics

The key optical diagnostic in the experiment, used for Rb density measurements, Rb polarimetry, and ^{3}He polarimetry, is Faraday rotation. The apparatus is shown schematically in Fig. 2. In the presence of a magnetic field, the Zeeman interaction causes a slight difference in the index of refraction for different light helicities, resulting in a rotation of the plane of polarization of light as it propagates through the cell. A similar effect occurs when the Rb electrons are spin polarized. A low-power tunable diode laser tuned approximately to 1000 GHz from the $P_{3/2}$ resonance at 780 nm is circularly polarized and modulated by a photoelastic modulator at a fre-

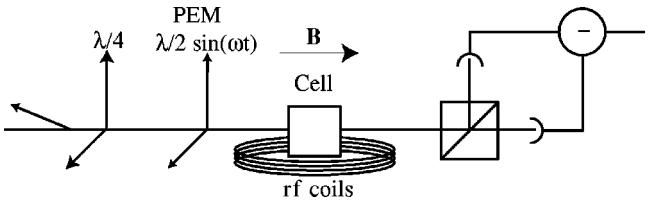

FIG. 2. Optical layout for absolute Rb density and polarization measurement. The arrows on the waveplate and the photoelatic modulator (PEM) show the principal axes of the birefringence.

quency $\omega = 2\pi \times 40$ kHz before entering the cell containing polarized atoms in a uniform longitudinal magnetic field (coils not shown). Low power is required to ensure that the probe does no optical pumping. A 780-nm bandpass interference filter passes the probe light while blocking out the intense light from the pumping laser for measurements taken with the pumping light on. The optical rotation is analyzed by a polarizing beam splitter cube and detected by a balanced photodiode pair. The difference of the photodiode signals v registers at the PEM modulation frequency ω, the polarization-induced Faraday rotation ϕ of the probe laser [26]: $v \propto \sin 2\phi$. The proportionality constant is determined by inserting a $\lambda/2$ plate and rotating it at a known angle.

1. Rb polarimetry

Absolute measurements of $\overline{P_{\mathrm{Rb}}}$ were made using rf spectroscopy on the Faraday rotation of a longitudinal probe. Recently, Young *et al.* [22,23] introduced a convenient method for measuring the absolute alkali polarization in optically pumped cells. They used a weak probe beam propagating perpendicular to the alkali polarization direction. Application of a transverse rf field at the Rb resonance frequency caused a polarization-dependent transmission modulated at the rf frequency. In such a way a set of rf resonances was observed that directly measured the populations in the various magnetic sublevels of the hyperfine structure of the ground-state atoms. A key feature of the method is that no vapor pressure measurement is required to get absolute polarization information.

For convenience, we use a variant of the above procedure, measuring Faraday rotation of a longitudinal probe as opposed to the transmission of a transverse probe. The application of a tranverse rf field at a Zeeman resonance of the Rb atoms causes a slight reduction in the spin polarization of the atoms. This in turn reduces the Faraday rotation of the probe beam. The signal is proportional to the square of the rf magnetic field and hence requires larger and more uniform rf fields than the transverse method of Young *et al*. The area A_{Fm} under a particular $(F, m) \rightarrow (F, m-1)$ line is proportional to the population difference of the two states multiplied by the square of the rf coupling between the two states:

$$A_{Fm} \propto B_{\mathrm{rf}}^2 [F(F+1) - m(m-1)](\rho_{Fm} - \rho_{Fm-1}). \quad (7)$$

Under the conditions of this experiment, the populations are well-characterized by a spin temperature [27] so that $\rho_{Fm} \propto \exp(\beta m)$, where $P_{\mathrm{Rb}} = \tanh(\beta/2)$. In addition, the alkali spin polarization is very close to 1 and in practice, unless we

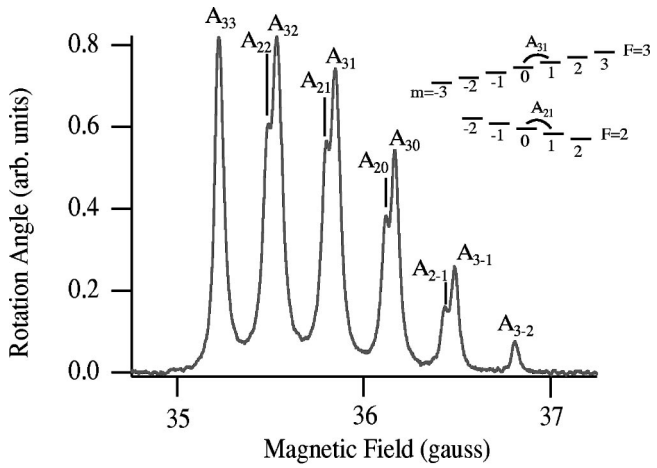

FIG. 3. ^{85}Rb polarization spectrum taken at 155°C and low Rb polarization. The relative areas A_{Fm} under the resonance peaks determine the Rb polarization. The A_{3m} and A_{2m} transitions are partially resolved. The inset shows the energy levels involved (not to scale), and example transitions.

purposely lower the polarization by reducing the pump laser power or tuning the pump-laser off-resonance, we observe only the A_{33}, A_{32}, A_{22} transitions of ^{85}Rb. The A_{32} and A_{22} transitions are only rarely resolved from each other. The measured ratio $r = A_{33}/(A_{32} + A_{22})$, in terms of which

$$P_{\mathrm{Rb}} = \left(\frac{7r-3}{7r+3}\right), \quad (8)$$

is therefore a useful and practical way to determine the polarization from spectra such as Fig. 4.

We generated the rf magnetic field using a six-turn circular coil mounted below the cell and driven from a programmable function generator as part of a tank circuit. We typically fixed the rf frequency at 16 MHz and swept the magnetic field from 35 G to 37 G, recording the Faraday rotation. Typical spectra are shown in Figs. 3 and 4. In Fig. 3 the Rb polarization has been purposely made small in order to see the various transitions. Under the actual conditions that the data were taken for this experiment, the Rb polarizations were very high. Only at the highest temperatures (>190°C) was the $A_{32} + A_{22}$ peak observable and thus over virtually the entire dataset discussed here the Rb polarization is essentially 100%. This is illustrated by the spectra in Fig. 4. Note that the resonance lines are considerably broader than in Fig. 3 due to a higher rate of spin-exchange collisions, except for the A_{33} peak that is narrowed for high polarizations [23]. We also periodically checked that the Rb polarization at the edge of the cell was high; in all cases presented here we found it to be in excess of 95% and even 1 mm from the outer edge of the cylinder.

2. Rb density measurements

We used both magnetic-field-induced and polarization-induced Faraday rotation to deduce the Rb density for this experiment. It is important to recognize that under high power pumping conditions there is substantial heating of the

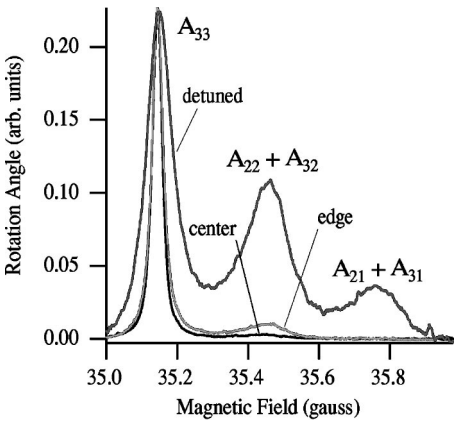

FIG. 4. ^{85}Rb polarization spectra taken at 183°C. The three cases shown are with the pump laser on resonance with the probe at the center and 1 mm from the edge of the cell, and with the laser off resonance. The three peaks, whose relative areas give the Rb polarization, correspond to the A_{33}, $A_{32}+A_{22}$, and $A_{31}+A_{21}$ transitions. The three spectra have been arbitrarily scaled to give the same height of the A_{33} peak.

gas [29] and the Rb density is often significantly higher than the external wall temperature would indicate. Thus is it important to be able to measure the Rb density with the pumping on and off. The two rotation methods allow us to accomplish this. With the pumping laser off, so that the Rb polarization is very small, we measure the Faraday rotation angle as a function of magnetic field [20], a technique whose accuracy and reliability we have recently studied at some length [21]. The rotation angle is, for detunings much greater than the atomic linewidth and hyperfine structure [28],

$$\theta_B = [\mathrm{Rb}]\frac{le^2\mu_B B}{18mhc}\left(\frac{4}{\Delta_{1/2}^2}+\frac{7}{\Delta_{3/2}^2}-\frac{2}{\Delta_{3/2}\Delta_{1/2}}\right), \tag{9}$$

where, for example, $\Delta_{3/2}=\nu-\nu_{3/2}$ is the detuning of the probe laser from the $6S_{1/2}\rightarrow 6P_{3/2}$ transition. Here also e is the electronic charge, μ_B is the Bohr magneton, m is the electron mass, h is Planck's constant, and c is the speed of light. Similarly, with the pumping laser on, the polarized Rb atoms produce a rotation

$$\theta_P = [\mathrm{Rb}]\frac{le^2}{6mc}\left(\frac{1}{\Delta_{3/2}}-\frac{1}{\Delta_{1/2}}\right)P_{\mathrm{Rb}}. \tag{10}$$

Since the Rb polarization is measured absolutely via the rf spectroscopy, the absolute rotation angle allows us to deduce the Rb density.

In practice, under conditions of small heating due to the pump laser we find that the two rotation methods usually agree to within 10%, giving us confidence in our density measurements. As a further check, we also measured the density using the more laborious technique of absorption spectroscopy on the $5s\rightarrow 6p$ resonances of Rb near 421 nm. The Rb 5s–5p resonance lines are not suitable for this since their large oscillator strengths makes them extremely optically thick under conditions of this experiment. We used a 150-mW, 825-nm Hitachi diode laser tuned by an external Littrow cavity to 842 nm. This light was frequency doubled by a Li:NbO_3 crystal, the output of which was coupled to the cell in the form of a narrow beam. After transmission through the cell, the blue light was isolated with an interference filter and a UV-sensitive photodiode. We then recorded transmission vs frequency as the light was tuned through the 421-nm resonances. The resulting absorption spectra were fit to determine the areas under the $5S_{1/2}\rightarrow 6P_{1/2,3/2}$ peaks. Then the areas were used with the known oscillator strengths to deduce the density. With the pump laser on (and hence heating) or off, the density deduced from absorption agreed with that from both types of Faraday rotation to typically 15%, limited by the accuracy of the absorption spectroscopy. The absorption spectroscopy accuracy was limited by small signals and beam alignment problems were associated with the frequency doubling.

We note that the consistency of the three Rb density measurements is also a check on our Rb polarimetry because the polarization rotation method is proportional to the product of the Rb density and polarization.

3. ^{3}He *polarimetry*

We make absolute ^{3}He polarization measurements using the Rb electron paramagnetic resonance (EPR) frequency shift method [24]. In the presence of polarized ^{3}He the Rb electrons experience a small effective magnetic field due to the Fermi-contact hyperfine interaction with the ^{3}He nucleus as the electrons penetrate the core of the ^{3}He atoms. The resulting frequency shift is a sensitive and accurate measure of the He polarization. With the pumping light on, we measure the shift $\Delta\nu$ in the Rb rf resonance frequency ν due to the polarization of ^{3}He [24]:

$$\Delta\nu = \frac{d\nu}{dB}\frac{8\pi}{3}\kappa\mu_K[\mathrm{He}]P_{\mathrm{He}} \tag{11}$$

$$= \left(1.13\frac{\mathrm{kHz}}{\mathrm{amagat}}\right)\kappa[\mathrm{He}]P_{\mathrm{He}}. \tag{12}$$

Here κ is the frequency shift enhancement factor and μ_K is the ^{3}He magnetic moment. For a nonspherical cell such as ours, the frequency shift is slightly modified by the nonuniform magnetic field produced inside the cell by the ^{3}He nuclei. For a cylindrical cell of radius a and length l, we use the method of magnetic scalar potential [30] to find that the average frequency shift enhancement on the cylinder axis is

$$\kappa = \kappa_0 + \frac{1}{2} - \frac{3}{2}\left[1+\frac{a}{l}-\sqrt{1+\left(\frac{a}{l}\right)^2}\right]. \tag{13}$$

For our cell with $a/l=0.46$, the correction term is $\kappa-\kappa_0=-0.04$. Romalis and Cates [24] recently measured $\kappa_0=4.52+0.009\,34T$, with T as the temperature in Celsius, to 1.5% accuracy.

The EPR system is similar to that of Romalis and Cates [24]. The rf coil is driven by a 3-MHz voltage-controlled oscillator with 2 kHz FM sidebands. The resulting 2-kHz modulation of the Faraday rotation is detected by a lock-in

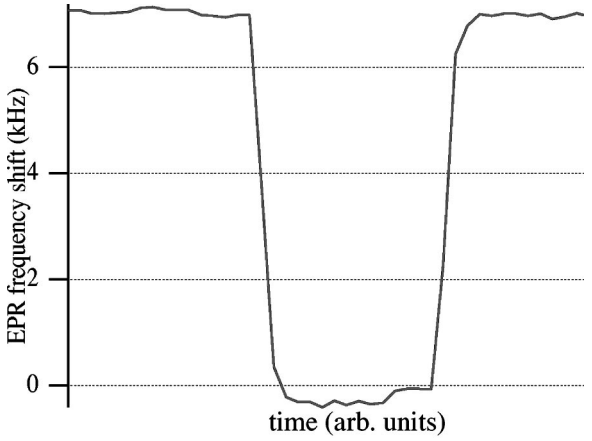

FIG. 5. EPR frequency as a function of time, showing the frequency shift upon AFP reversals. The ^{3}He polarization for these data is 69%.

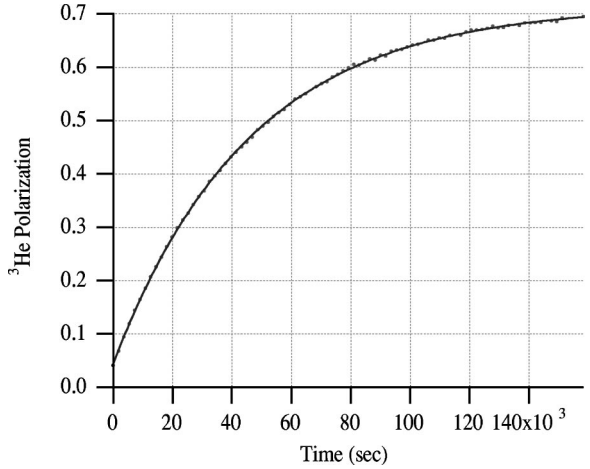

FIG. 6. Polarization buildup of ^{3}He at 170°C (raw data and exponential fit). The NMR is calibrated using the EPR frequency shift.

amplifier, producing the derivitive of the EPR line shape. A proportional/integral feedback circuit uses the lock-in output to adjust the rf frequency in order to keep the rf at the peak of the EPR resonance. A frequency counter samples the rf frequency every 1.0 sec. We then use adiabatic fast passage (Sec. III C) to reverse the ^{3}He spins, and observe the resulting change in the rf frequency, which is twice that of Eq. (12).

A sample EPR signal is shown in Fig. 5. Even with the modest 0.77 amagat ^{3}He density, the EPR shift is quite large and easily measurable. We note that we are routinely able to attain ^{3}He polarizations in excess of 70% in these experiments. The accuracy is limited by magnetic field drifts to typically 3%.

A potentially important uncertainty in the ^{3}He polarimetry is the accuracy of the measurement of the gas density. In order to check that the density as determined at the time of the cell filling was accurate, we have spectroscopically measured the Rb resonance-line absorption profiles at 780 nm and 795 nm at temperatures of typically 80°C where the lines are optically thin. We scanned a tunable diode laser across the resonance lines and measured absolute absorption as a function of frequency. Using the precision line-broadening parameters of Romalis *et al.* [31], and the known hyperfine and isotope structure, we fit the absorption spectra with the gas density as a free parameter. The measured gas density of 0.74 ± 0.2 amagat was in excellent agreement with the fill density.

4. Rb repolarization

The small ''repolarization'' of the Rb atoms produced by spin exchange with the polarized ^{3}He is measured by comparing the Faraday rotation of the repolarized atoms with the fully pumped atoms that result with the pump light on. The zero polarization rotation is determined by driving the Rb EPR resonance with a 2 Hz square-wave amplitude modulated rf pulse that strongly saturates the Rb resonance, making the Rb polarization zero.

The rf chopper method is also used to meaure Γ_{Rb}. After saturation with rf, the resulting Faraday rotation transient is detected and analyzed to obtain the decay rate γ of the slowest relaxation mode at low Rb polarization [18]. From this Γ_{Rb} is determined as $\Gamma_{\mathrm{Rb}} = \epsilon\gamma$. As a check, we also measure Γ_{Rb} by tuning the pump laser far off resonance so that $P_{\mathrm{Rb}} \ll 1$, and chop the pump laser on and off. Analyzing the transients in the same way gives results that agree with the rf chopper to better than 10%.

C. ^{3}He NMR

We perform NMR on the polarized ^{3}He using free-induction decay (FID) with a small surface coil. The 1.3-cm-diameter coil has 320 turns and a Q of 15 at 24.5 kHz. A resonant pulse at 24.5 kHz tips ^{3}He nuclei at the surface of the cell by a small angle. The resulting precession of nuclei is then detected with the same coil and analyzed to determine its initial amplitude. Using the shim turns on the Helmholtz coils to minimize magnetic field gradients, we thereby lengthen the transverse relaxation rate and typically attain transverse relaxation times $T2 \sim 170$ msec.

We determine Γ_{He} using time dependence of NMR free-induction decays, both in the presence and absence of pumping light. Due to the long relaxation times for ^{3}He, we take an FID sample once every 30 min, and normally observe for two to three time constants so that the ^{3}He polarization nearly reaches equilibrium. With the magnetic field stabilization on, we get excellent signal-to-noise ratio on the ^{3}He transients. Figure 6 shows an example. Note that it is not necessary to start from zero polarization in order to determine the time constant for the ^{3}He relaxation. The loss per FID pulse is measured to be $<0.005\%$ by repeating a sequence of FID pulse once every 7 sec for 10 min at room temperature.

Though we could detect the ^{3}He polarization using adiabatic fast passage (AFP) [24,32], we instead simply use it to reverse the ^{3}He spins for the EPR ^{3}He polarimetry. As a strong transverse rf field is swept through resonance, the precession of the nuclei about the effective magnetic field in the rotating frame causes the nuclei to flip direction. The AFP

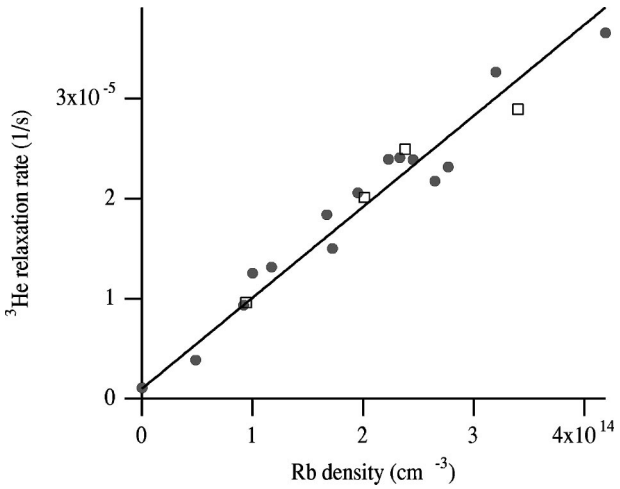

FIG. 7. ^{3}He spin-relaxation rate as a function of Rb density. The circles are the points taken with the pumping laser on, the squares have the pumping laser off.

coils are 20 turns with a 22 cm diameter, and driven by a programmable frequency source. With the magnetic field held at 5.65 G, we slowly sweep the AFP drive frequency from 11 950 Hz to 26 050 Hz over a time of 5.9 sec. The pickup coil is tuned off resonance during the AFP sweep. Repeating the AFP flips many times, we determine a loss per flip of about 0.5%.

IV. RESULTS

Figure 7 shows the ^{3}He relaxation rate as a function of Rb density. The bulk of the data were taken with the pumping on, but at a few temperatures we also measured the relaxation rate with the laser off. At a given temperature, the rate with the laser on was higher than with it off, typically by 30%, but the figure shows that the difference is entirely due to a difference in the Rb density. The slope of the line gives a rate coefficient of $9.1\pm0.3\times10^{-20}$ cm^3/s.

Figure 8 shows the spin-exchange rate coefficients (actually $k_a-k_b/2$), as deduced by the repolarization and rate-balance methods, for a series of data runs. The individual points show fluctuations about the mean of about 20%, but the statistical averages of the two methods (assuming no temperature dependence of the rate coefficient) give $7.2\pm0.4\times10^{-20}$ cm^3/s for the rate-balance method and $7.0\pm0.2\times10^{-20}$ cm^3/s for the repolarization method.

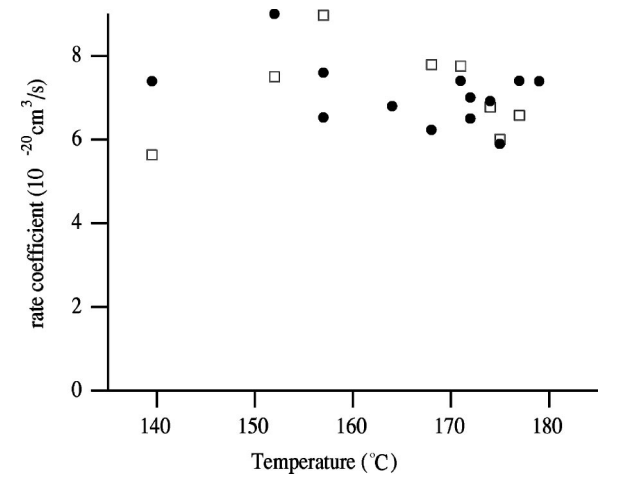

FIG. 8. Spin-exchange rate coefficients deduced using the repolarization method (circles) and the rate-balance method (open squares).

We also measured the spin-exchange rate coefficients with a second cell whose room temperature wall relaxation time was only 6.7 h. It was not possible to attain high He polarizations with this cell, but the deduced spin-exchange rate coefficients agreed well with the other cell: $6.7\pm0.2\times10^{-20}$ cm^3/s for the rate-balance method and $6.3\pm0.3\times10^{-20}$ cm^3/s for the repolarization method.

The close agreement between the results of the repolarization and rate-balance methods is a strong evidence that the systematic errors in the experiment are well controlled. The repolarization method uses the measured values of Rb relaxation rate, Rb repolarization, ^{3}He polarization, and He density. The rate-balance method requires measurements of the ^{3}He relaxation rate, ^{3}He polarization, Rb polarization (very close to 1 for our experiment), and Rb density. The only common measured quantity is the absolute ^{3}He polarization, which occurs in the numerator of the rate-balance expression [Eq. (4)] and the denominator of the repolarization expression [Eq. (6)]. Thus the systematic errors in the two methods should be very different.

The significantly larger value deduced with the relaxation-rate method, as compared to the repolarization and rate-balance methods, indicates the presence of a temperature dependent wall-relaxation rate and/or significant anisotropic spin-exchange contributions. In order to explain the data, the wall-relaxation mechanism must produce a relaxation rate that varies linearly with the Rb density, implying a temperature dependence similar to that of the saturated Rb vapor pressure. Alternatively, anisotropic spin exchange could also be present, though it would need to be much larger than that estimated by Walter *et al.* [17]. Assuming anisotropic spin exchange is responsible for the entire difference would give, using Eq. (2) and Eq. (4), $k_b<1.4\pm0.6\times10^{-20}$ cm^3/s, nearly an order of magnitude larger than the 1.7×10^{-21} cm^3/s predicted by Walter *et al.*

Comparison of the spin-exchange rate coefficients measured here (both cells combined) with previous results is done in Table I. The measurements that use the relaxation-rate method vary widely and are in general larger than those obtained with other methods. The variation may be a result of the different walls used in the three experiments, or inaccuracies in determining vapor pressures in the previous experiments, or both.

Both the current repolarization and rate-balance results reported here are in excellent agreement with the Baranga *et al.* [15] result of $6.7\pm0.6\times10^{-20}$ cm^3/s, and also in excellent agreement with the theoretical prediction of 5.6×10^{-20} cm^3/s by Walter *et al.* [17]. Since the calculation of both the isotropic and anisotropic spin-exchange rates uses the same wave functions, this gives support for the reliablity of the Walter estimates, and makes it probable that the explanation for the higher results for the relaxation-rate method

TABLE I. Measured spin-exchange rate coefficients using various methods. The relaxation-rate method results are likely contaminated by wall effects, while the repolarization and rate-balance methods require no understanding of the wall. The results quoted for this work are the combined results for two different cells, and the errors are statistical.

References	Method	Result (10^{-20} cm^3/s)
[16]	Relaxation rate	12 ± 2
[10]	Relaxation rate	6.2 ± 2
This work	Relaxation rate	9.1 ± 0.3
[15]	Repolarization	6.7 ± 0.6
This work	Repolarization	6.8 ± 0.2
This work	Rate balance	6.8 ± 0.2

is that there is a temperature-dependent wall-relaxation mechanism that scales closely with the Rb density.

In this work we have achieved He polarizations in excess of 70%. This value is consistent with the ratio of the spin-exchange and spin-relaxation rates,

$$P_{\mathrm{He}}=\frac{(k_a-k_b/2)[\mathrm{Rb}]}{\Gamma_{He}}P_{\mathrm{Rb}}. \tag{14}$$

Experimentally, we find that Γ_{He} is linear in Rb density, with slope determined by the spin-relaxation method. Thus the maximum achievable polarization is the ratio of the rate coefficient determined by repolarization or rate balance, divided by the rate coefficient for the ^{3}He relaxation. The value so obtained, 0.74 ± 0.03, is consistent with the maximum ^{3}He polarizations we have observed.

In summary, we have measured the spin-exchange rate coefficient for the important Rb-^{3}He system, which is widely used for producing spin-polarized ^{3}He. We have introduced a ''rate-balance'' method for measuring the rate coefficient that does not depend on assumptions about other ^{3}He relaxation mechanisms, in particular the wall relaxation. It gives excellent agreement with the ''repolarization'' method of Baranga *et al.* [15]. We have shown that the ^{3}He spin-relaxation rate increases with increasing Rb density at a rate that is significantly greater than what can be accounted for by spin exchange. It is vital to understand the source of this wall relaxation (or anisotropic spin exchange) in order to understand why experiments have been unable to attain ^{3}He polarizations much in excess of 70%.

ACKNOWLEDGMENTS

This work was supported by the National Science Foundation. Tom Gentile, Dennis Rich, and Alan Thompson of NIST provided the cells, and we benefited from many helpful discussions with them as well. We also acknowledge discussions with S. Kadlecek and I. Nelson of Amersham Health.

APPENDIX

The derivation of the basic equation of the repolarization method, Eq. (6), assumed that the Rb spin relaxation is dominated by electron randomization processes, as first pointed out by Baranga *et al.* [15]. At high pressures and relatively low densities, such that the relaxation due to Rb-Rb interactions can be neglected, the assumption of electron randomization is justified since the relaxation occurs in Rb-He binary collisions whose duration is so short that there is negligible precession of the nucleus during the collision. But when Rb-Rb relaxation is important we recently discovered that there are other spin-relaxation mechanisms that arise from the formation of triplet [33,34] and singlet [35] Rb_2 molecules. We argue here that as long as Γ_{Rb} is properly interpreted, Eq. (6) should still hold even when such processes are present.

The spin-relaxation due to molecular processes is complicated, but can be approximated at low Rb polarization by replacing $\Gamma_{\mathrm{Rb}}\langle S_z\rangle_0\rightarrow\Gamma_S\langle S_z\rangle_0+\Gamma_F\langle F_z\rangle_0$ in Eq. (5). Here Γ_S denotes the relaxation rate arising from binary collisions, and Γ_F the relaxation rate from molecules. As long as spin-conserving Rb-Rb spin-exchange collisions occur at a much greater rate than the spin-relaxing collisions, a condition well satisfied in our experiments, then for small polarizations the well-known approximation $\langle F_z\rangle_0=\epsilon\langle S_z\rangle_0$ holds, with the ''slowing-down factor'' $\epsilon=10.8$ for Rb vapor of natural isotopic composition [8,18]. The slowing-down factor accounts for the storage of most of the angular momentum of the Rb vapor in the nuclei.

With the above modifications and assumptions, Eq. (5) predicts that the Rb polarization decays at a rate $\gamma=\Gamma_F+\Gamma_S/\epsilon$, and that the steady-state Rb polarization in the absence of optical pumping is $P_{\mathrm{Rb0}}=(k_a-k_b/2)P_{\mathrm{He0}}[\mathrm{He}]/(\epsilon\gamma)$. Identifying $\Gamma_{\mathrm{Rb}}=\epsilon\gamma$ gives Eq. (6). Thus Γ_{Rb} should be obtained from the product of the measured Rb relaxation rate and the slowing-down factor. With this procedure the value of the spin-exchange rate coefficient deduced from Eq. (6) should be insensitive to the mechanism for the electron spin relaxation.

[1] H. Middleton *et al.*, Magn. Reson. Med. **33**, 271 (1995).

[2] M. Salerno, T.A. Altes, J.R. Brookeman, E. de Lange, and J.P.I. Mugler, Magn. Reson. Med. **46**, 667 (2001).

[3] W. Xu *et al.*, Phys. Rev. Lett. **85**, 2900 (2000).

[4] G. Jones, T. Gentile, A. Thompson, Z. Chowdhuri, M. Dewey, W. Snow, and F. Wietfeldt, Nucl. Instrum. Methods Phys. Res. A **440**, 772 (2000).

[5] D. Bear, R.E. Stoner, R.L. Walsworth, V.A. Kostelecky, and C.D. Lane, Phys. Rev. Lett. **85**, 5038 (2000).

[6] M.F. Hsu, G.D. Cates, I. Kominis, I.A. Aksay, and D.M. Dabbs, Appl. Phys. Lett. **77**, 2069 (2000).

[7] D.R. Rich, T.R. Gentile, T.B. Smith, A.K. Thompson, and G.L. Jones, Appl. Phys. Lett. **80**, 2210 (2002).

[8] T. Walker and W. Happer, Rev. Mod. Phys. **69**, 629 (1997).

[9] K.P. Coulter, T.E. Chupp, A.B. McDonald, C.D. Bowman, J.D. Bowman, J.J. Szymanski, V. Yuan, G.D. Cates, D.R. Benton, and E.D. Earle, Nucl. Instrum. Methods Phys. Res. A **288**, 463 (1990).

[10] B. Larson, O. Husser, P.P.J. Delheij, D.M. Whittal, and D. Thiessen, Phys. Rev. A **44**, 3108 (1991).
[11] B. Chann, E. Babcock, D. Rich, A. Thompson, T. Smith, L.W. Anderson, T. Gentile, and T.G. Walker (unpublished).
[12] T.R. Gentile and R.D. McKeown, Phys. Rev. A **47**, 456 (1993).
[13] J. Becker *et al.*, Nucl. Instrum. Methods Phys. Res. A **402**, 327 (1998).
[14] T. Gentile, D.R. Rich, A.K. Thompson, W.M. Snow, and G.L. Jones, J. Res. Natl. Inst. Stand. Technol. **106**, 706 (2001).
[15] A. Ben-Amar Baranga, S. Appelt, M.V. Romalis, C.J. Erickson, A.R. Young, G.D. Cates, and W. Happer, Phys. Rev. Lett. **80**, 2801 (1998).
[16] K.P. Coulter, A.B. McDonald, W. Happer, T.E. Chupp, and M.E. Wagshul, Nucl. Instrum. Methods Phys. Res. A **270**, 90 (1988).
[17] D.K. Walter, W. Happer, and T.G. Walker, Phys. Rev. A **58**, 3642 (1998).
[18] S. Appelt, A. Ben-Amar Baranga, C.J. Erickson, M.V. Romalis, A.R. Young, and W. Happer, Phys. Rev. A **58**, 1412 (1998).
[19] N. Newbury, A.S. Barton, G.D. Cates, W. Happer, and H. Middleton, Phys. Rev. A **48**, 4411 (1993).
[20] Z. Wu, M. Kitano, W. Happer, M. Hou, and J. Daniels, Appl. Opt. **25**, 4483 (1986).
[21] E. Vliegen, S. Kadlecek, L.W. Anderson, and T.G. Walker, Nucl. Instrum. Methods Phys. Res. A **460**, 444 (2001).
[22] A. Young, S. Appelt, A. Ben-Amar-Baranga, C. Erickson, and W. Happer, Appl. Phys. Lett. **70**, 3081 (1997).
[23] A. Ben-Amar Baranga, S. Appelt, C. Erickson, A. Young, and W. Happer, Phys. Rev. A **58**, 2282 (1998).
[24] M. Romalis and G. Cates, Phys. Rev. A **58**, 3004 (1998).
[25] B. Chann, I. Nelson, and T.G. Walker, Opt. Lett. **25**, 1352 (2000).
[26] J.C. Kemp (unpublished).
[27] L.W. Anderson, F.M. Pipkin, and J.C. Baird, Phys. Rev. **116**, 87 (1959).
[28] The last term in this equation was erroneously omitted in Ref. [21]. As pointed out to us by Fortson, it arises from Zeeman mixing of the fine-structure states. It is negligible for the small detunings (relative to the fine-structure splitting) used in this work, but accounts for small systematic discrepancies observed in Ref. [21].
[29] D.K. Walter, W.M. Griffith, and W. Happer, Phys. Rev. Lett. **86**, 3264 (2001).
[30] J.D. Jackson, *Classical Electrodynamics* (Wiley, New York, 1975).
[31] M.V. Romalis, E. Miron, and G.D. Cates, Phys. Rev. A **56**, 4569 (1997).
[32] C.P. Slichter, *Principles of Nuclear Magnetism* (Oxford University Press, Oxford, 1961).
[33] S. Kadlecek, L.W. Anderson, and T. Walker, Phys. Rev. Lett. **80**, 5512 (1998).
[34] C.J. Erickson, D. Levron, W. Happer, S. Kadlecek, B. Chann, L.W. Anderson, and T.G. Walker, Phys. Rev. Lett. **85**, 4237 (2000).
[35] S. Kadlecek, L.W. Anderson, C.J. Erickson, and T.G. Walker, Phys. Rev. A **64**, 052717 (2001).